nature chemistry

ARTICLES

https://doi.org/10.1038/s41557-022-00967-4

Check for updates

In situ electrochemical recomposition of decomposed redox-active species in aqueous organic flow batteries

Yan Jing[1,8], Evan Wenbo Zhao[2,5,8], Marc-Antoni Goulet[3,6,8], Meisam Bahari[3], Eric M. Fell[3], Shijian Jin[3], Ali Davoodi[3,4,7], Erlendur Jónsson[2], Min Wu[3], Clare P. Grey[2]✉, Roy G. Gordon[1,3]✉ and Michael J. Aziz[3]✉

Aqueous organic redox flow batteries offer a safe and potentially inexpensive solution to the problem of storing massive amounts of electricity produced from intermittent renewables. However, molecular decomposition represents a major barrier to commercialization—and although structural modifications can improve stability, it comes at the expense of synthetic cost and molecular weight. Now, utilizing 2,6-dihydroxy-anthraquinone (DHAQ) without further structural modification, we demonstrate that the regeneration of the original molecule after decomposition represents a viable route to achieve low-cost, long-lifetime aqueous organic redox flow batteries. We used in situ (online) NMR and electron paramagnetic resonance, and complementary electrochemical analyses to show that the decomposition compound 2,6-dihydroxy-anthrone (DHA) and its tautomer, 2,6-dihydroxy-anthranol (DHAL) can be recomposed to DHAQ electrochemically through two steps: oxidation of $DHA(L)^{2-}$ to the dimer $(DHA)_2^{4-}$ by one-electron transfer followed by oxidation of $(DHA)_2^{4-}$ to $DHAQ^{2-}$ by three-electron transfer per DHAQ molecule. This electrochemical regeneration process also rejuvenates the positive electrolyte—rebalancing the states of charge of both electrolytes without introducing extra ions.

Organic molecules, when used for aqueous redox flow batteries, hold great promise to greatly lower the levelized costs of electricity storage while also outperforming their inorganic counterparts; this is because they possess considerable structural diversity and tunability, and are composed of earth-abundant elements[1,2]. However, the instability of organic molecules under the harsh electrochemical conditions found in aqueous organic redox flow batteries is one of the biggest obstacles for their commercialization[3]. Although extremely stable redox organic molecules have been synthesized, this has come at the expense of increased synthetic cost and molecular weight[4–10].

2,6-Dihydroxyanthraquinone (DHAQ), although an inexpensive molecule (estimated cost: US$4.02 per kg, US$23.70 per kAh)[11], shows a fast temporal fade rate due to the instability of the reduced DHAQ ($DHAQ^{4-}$), which reacts to form redox-inactive 2,6-dihydroxyanthrone (DHA) and its tautomer 2,6-dihydroxyanthranol (DHAL)[12,13]. Goulet, Tong and colleagues reduced the reaction rate by restricting the negative electrolyte (negolyte) state of charge (SOC) and converted a substantial amount of the $DHA(L)^{2-}$ back to $DHAQ^{2-}$ by aeration of the negolyte, thereby extending the overall lifetime of the battery[12]. $DHAQ^{4-}$ can also be electrochemically reduced[13,14] to form $DHA(L)^{2-}$, which can be subsequently electrochemically oxidized to the dimer $(DHA)_2^{4-}$. As the direct electrosynthesis of the water-soluble anthraquinones from their anthracene precursors has already been demonstrated via multiple-electron transfer processes[15], we set out to exploit and build on the above insight to study the viability of electrochemically regenerating DHAQ from the redox-inactive (reduced) compounds. In situ NMR and electron paramagnetic resonance (EPR) metrologies are used to observe the stepwise conversions in real time (that is, $DHAQ^{2-}$ to $DHAQ^{4-}$, to $DHA(L)^{2-}$, then to its dimer $(DHA)_2^{4-}$ and finally back to $DHAQ^{2-}$) by adjusting cell voltages ad hoc (Fig. 1a,b). The conversion from $DHA(L)^{2-}$ to $DHAQ^{2-}$ is further confirmed by utilizing a $DHA(L)^{2-}$|$[Fe(CN)_6]^{3-/4-}$ flow cell, and corresponding oxidation potentials are determined by an embedded reference electrode. In combination with the demonstrated electrochemical reduction, this study demonstrates the full loop of DHAQ electrochemical molecular conversions and shows that anthraquinone redox flow batteries can be the electrochemically regenerated. The capacity fade rate of the full cell was decreased by more than an order of magnitude by applying the electrochemical regeneration method. The resulting capacity fade rate of 0.38% per day at 100% SOC is lower than the value of 0.49% per day previously reported by constricting the SOC range to 80%[12,16]. The method thus achieves a slightly better battery lifetime while enabling the battery to use the full SOC of the DHAQ electrolyte, effectively reducing the capital cost of this electrolyte by 20%.

Results and discussion

In situ ^{1}H NMR tracking during the electrochemical redox reactions. A series of NMR and electrochemical experiments was

[1]Department of Chemistry and Chemical Biology, Harvard University, Cambridge, MA, USA. [2]Yusuf Hamied Department of Chemistry, University of Cambridge, Cambridge, UK. [3]John A. Paulson School of Engineering and Applied Sciences, Harvard University, Cambridge, MA, USA. [4]Materials and Metallurgical Engineering Department, Faculty of Engineering, Ferdowsi University of Mashhad (FUM), Mashhad, Iran. [5]Present address: Magnetic Resonance Research Center, Institute for Molecules and Materials, Radboud University Nijmegen, Nijmegen, the Netherlands. [6]Present address: Department of Chemical and Materials Engineering, Concordia University, Montreal, Quebec, Canada. [7]Present address: Sichuan University-Pittsburgh Institute, Sichuan University, Chengdu, China. [8]These authors contributed equally: Yan Jing, Evan Wenbo Zhao, Marc-Antoni Goulet. ✉e-mail: cpg27@cam.ac.uk; gordon@chemistry.harvard.edu; maziz@harvard.edu

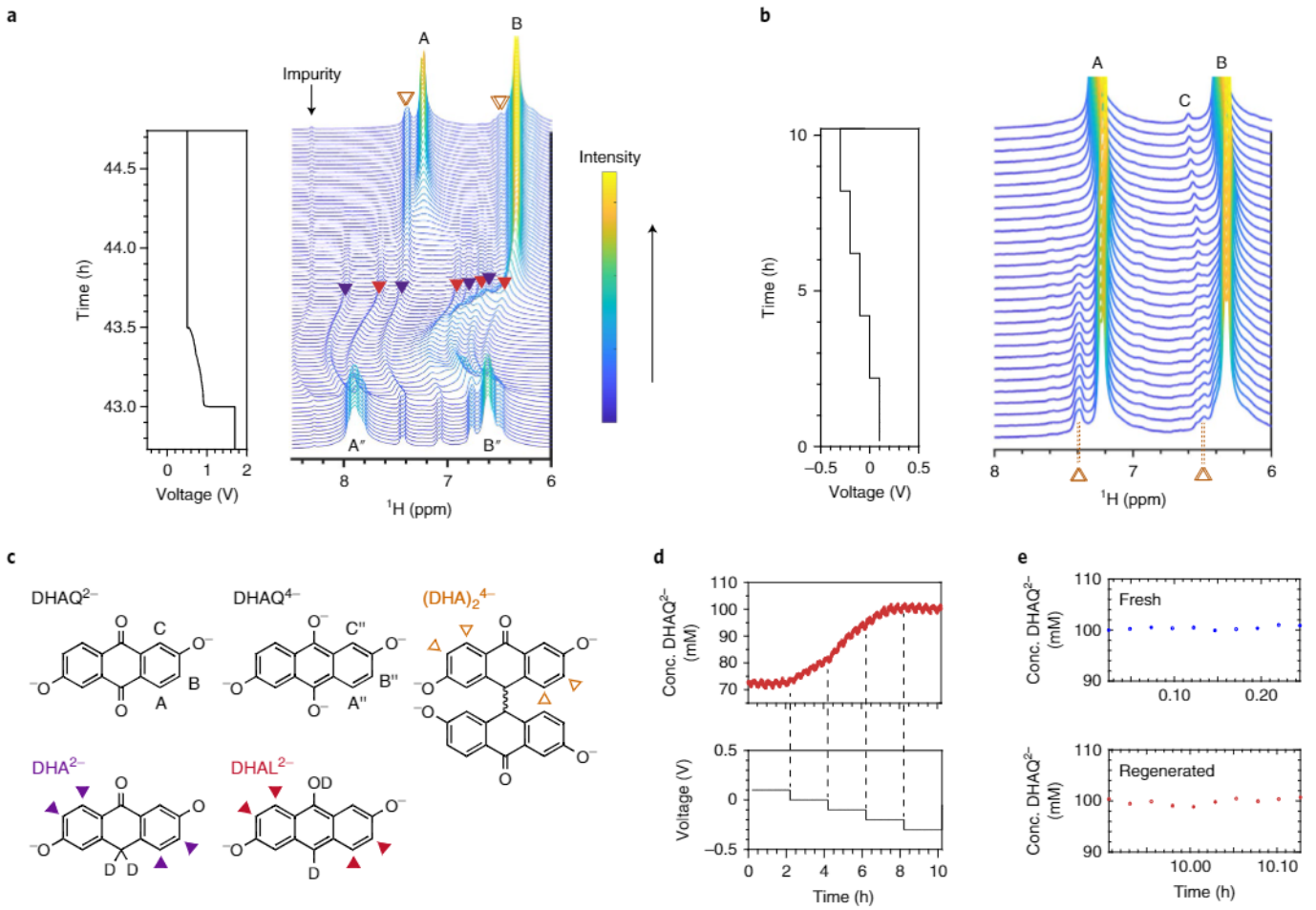

Fig. 1 | In situ ^{1}H NMR spectra acquired during electrochemical cycling. a, Voltage (left) and corresponding in situ ^{1}H NMR spectra of the aromatic region of the negolyte (right). The voltage was held at 1.7 V and then a constant discharge current of −30 mA cm^{-2} was applied, followed by a voltage hold at 0.5 V. The colour bar indicates the intensity of ^{1}H resonances. The temporal voltage profile for the electrochemical cycling experiment is shown in Supplementary Fig. 1. **b**, In situ ^{1}H NMR spectra acquired during a stepped voltage-hold experiment. **c**, Molecular structures of the $DHAQ^{2-}$, $DHAQ^{4-}$, DHA^{2-}, $DHAL^{2-}$ and $(DHA)_2^{4-}$ anions. **d**, Concentration of $DHAQ^{2-}$ anions (top) and the voltage of the battery (bottom) as a function of time during the stepped voltage-hold experiment. **e**, Concentrations of $DHAQ^{2-}$ anions in a fresh uncycled negolyte solution (top) and at the end of the voltage hold at −0.3 V (bottom). The concentrations were calculated from the intensities of DHAQ signal A. The battery used in these experiments is composed of 25 ml, 100 mM DHAQ in the negolyte and a mixture of 50 ml, 200 mM $K_4[Fe(CN)_6]$ and 100 mM $K_3[Fe(CN)_6]$ in the positive electrolyte (posolyte); 1.2 M and 1 M KOH dissolved in D_2O were used as solvents for the negolyte and posolyte, respectively, and Nafion 117 was used as the membrane. The proton resonances are labelled A, B (and C) for DHAQ, with double-prime labels indicating the same protons in the doubly reduced anions. The solid purple, red and hollow brown triangles in **a** and **c** highlight the signals and corresponding positions of the protons on the aromatic rings of the decomposition products DHA^{2-}, $DHAL^{2-}$ and $(DHA)_2^{4-}$, respectively.

performed to explore the reactions outlined in Fig. 2a. Following an initial charge of a full cell at 30 mA cm^{-2}, which was performed to reduce the redox-active components in the negolyte (namely 100 mM DHAQ), the voltage of the battery was held at 1.7 V for 42 h while monitoring the in situ ^{1}H NMR spectra (Fig. 1a). The ^{1}H NMR signals A″ and B″ of the $DHAQ^{4-}$ anions are clearly visible along with weaker signals from the $DHA(L)^{2-}$ at 6.49, 6.57, 6.77, 7.08, 7.43, 7.82 and 7.95 ppm. Note that DHA^{3-} and $DHAL^{3-}$ were proposed as resonance structures in our previous work[12,13]. As eight doublets were observed in this work (Fig. 1a and Supplementary Fig. 2c), we propose that DHA^{3-} and $DHAL^{3-}$ are in fact deuterated to form the DHA^{2-} and $DHAL^{2-}$ anions, which are tautomers[17]. The cell was then discharged at a constant current of −30 mA cm^{-2}, the voltage decreasing rapidly to 0.9 V and then dropping more gradually to a cut-off voltage of 0.5 V. This was followed by a voltage hold at 0.5 V for 7.4 h. Note that a previously reported second voltage plateau at approximately 0.7 V during discharge[14]—corresponding to the oxidation of $DHA(L)^{2-}$ to $(DHA)_2^{4-}$—was not observed due to the high overpotential caused by the thick Nafion 117 membrane used in this experiment. During discharge, the fast electron transfer between $DHAQ^{\bullet 3-}$ and $DHAQ^{4-}$ anions causes broadening of the $DHAQ^{4-}$ peaks, A″ and B″, allowing the DHA^{2-} and $DHAL^{2-}$ signals (marked with solid purple and red triangles, respectively) to be seen more clearly as they remain unaffected by this broadening mechanism[13,14]. The shift of all of these signals is caused by the change of the bulk magnetization of electrolyte solution as $DHAQ^{\bullet 3-}$ anions are produced from $DHAQ^{4-}$ oxidation and then further oxidized to $DHAQ^{2-}$. During the voltage hold at 0.5 V, the $DHAQ^{2-}$ A and B peaks, and new signals at 6.36, 6.41, 7.40 and 7.41 ppm (marked with hollow brown triangles), grow in intensity, accompanied by the decrease of signal intensities of $DHA(L)^{2-}$. The new peaks are assigned to $(DHA)_2^{4-}$ on the basis of an in situ two-dimensional ^{1}H homonuclear correlation spectrum (COSY), as shown in Supplementary Fig. 2. $DHA(L)^{2-}$ can therefore be

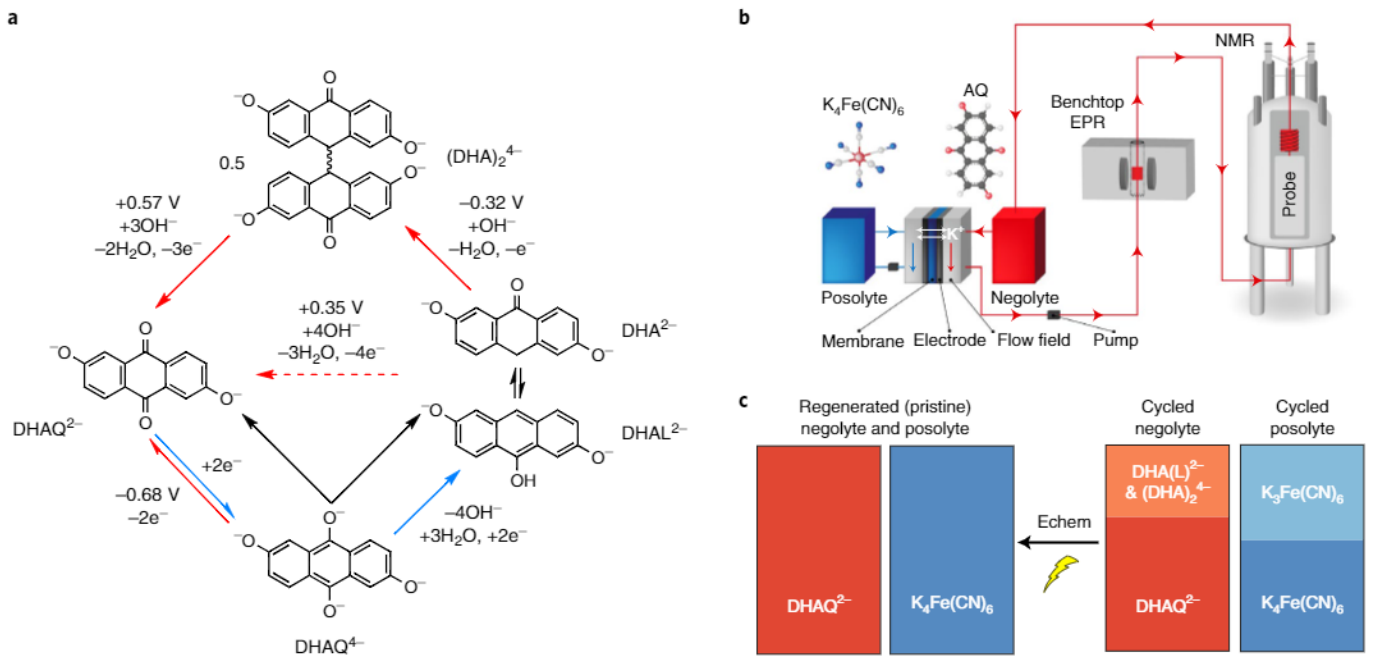

Fig. 2 | Electrochemically rejuvenating a DHAQ|Fe(CN)$_6$ flow battery. a, Potential-driven DHAQ-related molecular conversions at pH 14 explored in this work. **b**, In situ NMR and EPR metrologies used to monitor electrochemical conversions. The 'AQ' in the schematic represents 2,6-dihydroxyanthraquinone (DHAQ). **c**, A rejuvenated DHAQ flow cell resulting from the electrochemical regeneration. Negolyte denotes the negative electrolyte; posolyte denotes the positive electrolyte. The potentials, E (versus SHE) in **a** near the solid red and blue arrows are experimentally determined with an embedded reference electrode; the potential near the dashed red arrow is calculated from the equation $E = \Delta G/-nF$, where n is the number of electrons transferred in the reactions and F is the Faraday constant. The change in Gibbs free energy of the overall reaction (DHA^{2-} to $DHAQ^{2-}$) is the sum of the changes in Gibbs free energy of the two reactions (DHA^{2-} to $(DHA)_2^{4-}$ and $(DHA)_2^{4-}$ to $DHAQ^{2-}$), where the Gibbs free energy is calculated by $\Delta G = -nFE$. The reduction of $DHAQ^{4-}$ to $DHAL^{2-}$ proceeds either chemically via a disproportionation of $DHAQ^{4-}$:$2DHAQ^{4-} + 3H_2O \rightarrow DHAQ^{2-} + DHAL^{2-} + 4OH^-$, or electrochemically. Note that $DHAL^{2-}$ can tautomerize to DHA^{2-} and the electrochemical reaction is probably a multistep process (see text). The red arrows indicate electrochemical oxidations, the blue arrows indicate electrochemical reductions and the black arrows indicate chemical reactions. The equilibrium arrows indicate reversible reactions. For simplicity, $Fe(CN)_6$ refers to either $[Fe(CN)_6]^{3-}$ or $[Fe(CN)_6]^{4-}$, or a mixture of both.

electrochemically oxidized to $(DHA)_2^{4-}$ at $\leq$0.5 V versus the $K_4[Fe(CN)_6]/K_3[Fe(CN)_6]$ couple.

To test whether $(DHA)_2^{4-}$ can be oxidized further, the voltage of the battery was decreased from 0.1 V to −0.3 V in 0.1 V steps, holding for 2 h at each voltage step. The corresponding in situ ^{1}H NMR spectra are shown in Fig. 1b. The intensity of the $(DHA)_2^{4-}$ dimer signals (marked with hollow brown triangles) starts to decrease at 0.1 V with the rate of intensity drop increasing as the voltage is held at a more negative value. The $(DHA)_2^{4-}$ signals disappear completely at −0.2 V (Supplementary Fig. 2e), which is accompanied by an increase of $DHAQ^{2-}$ signal intensities. This observation indicates that $(DHA)_2^{4-}$ has been electrochemically oxidized to $DHAQ^{2-}$, following our proposed molecular conversion (Fig. 2a). Note that the corresponding oxidation potentials cannot be determined from this full cell experiment, due to the Nernstian shift of the potentials of the posolyte and negolyte as functions of state of charge and the large overpotentials caused by the internal resistances. The shift of signals A, B and C at −0.3 V was caused by the change in the bulk magnetization of electrolyte solution, now induced by the oxidation of the ferrocyanide ions that have crossed the membrane into the negolyte[18]. Note that the C/C″ signals are always weak due H/D exchange at the C position[13,14].

The concentration of $DHAQ^{2-}$ as a function of voltage has been quantified (Fig. 1d). It remains at 72 mM at 0.1 V and starts to increase to 80 mM, 95 mM and 100 mM at 0 V, −0.1 V and −0.2 V, respectively. A comparison of the initial concentration of $DHAQ^{2-}$ (that is, 100.4 mM ± 0.25 mM) with the concentration after electrochemical recomposition (that is, 99.9 mM ± 0.44 mM) is shown in Fig. 1e. A volumetric loss of 2 ml from the negolyte solution (DHAQ) was measured at the end of the experiment. The loss could be caused by water cross-over from the negolyte to the posolyte and water splitting in the negolyte. Taking into account this volumetric loss, a lower limit of concentration for recovered $DHAQ^{2-}$ is 91.9 mM. A second experiment with a voltage hold down to −0.6 V has also shown a substantial recomposition of $DHAQ^{2-}$ anions (Supplementary Fig. 3). Furthermore, the degradation products $DHA(L)^{2-}$ were produced again when the voltage was increased to 1.7 V (Supplementary Fig. 3), demonstrating the circularity of the electrochemical reactions from $DHAQ^{2-}$ to $DHA(L)^{2-}$, to $(DHA)_2^{4-}$ and back to $DHAQ^{2-}$ at different potentials, as illustrated in Fig. 2a. Note that no degradation products were detected at the end of the recomposition step within the detection limit of 0.4 mM for the in situ NMR method (see the 'Pseudo-2D NMR' section in the Methods for details), suggesting that if any degradation product persists, it is NMR-silent or below the instrument detection limit. This possibility is discussed further later.

Electrochemical and chemical oxidation of $DHA(L)^{2-}$. To further explore the recomposition of $DHAQ^{2-}$ as revealed by the in situ ^{1}H NMR spectra, we synthesized[12] DHA(L) and built a separate $DHA(L)^{2-}|[Fe(CN)_6]^{3-/4-}$ flow cell. By applying constant current to the negolyte versus $[Fe(CN)_6]^{3-/4-}$, we first oxidized $DHA(L)^{2-}$ to $(DHA)_2^{4-}$ via a one-electron transfer and then oxidized $(DHA)_2^{4-}$ to pure $DHAQ^{2-}$ via a three-electron transfer, with a close to quantitative yield (>95%) (Fig. 3a). The ex situ ^{1}H NMR spectra (Fig. 3b) show that the peaks from $DHA(L)^{2-}$ completely disappear and the

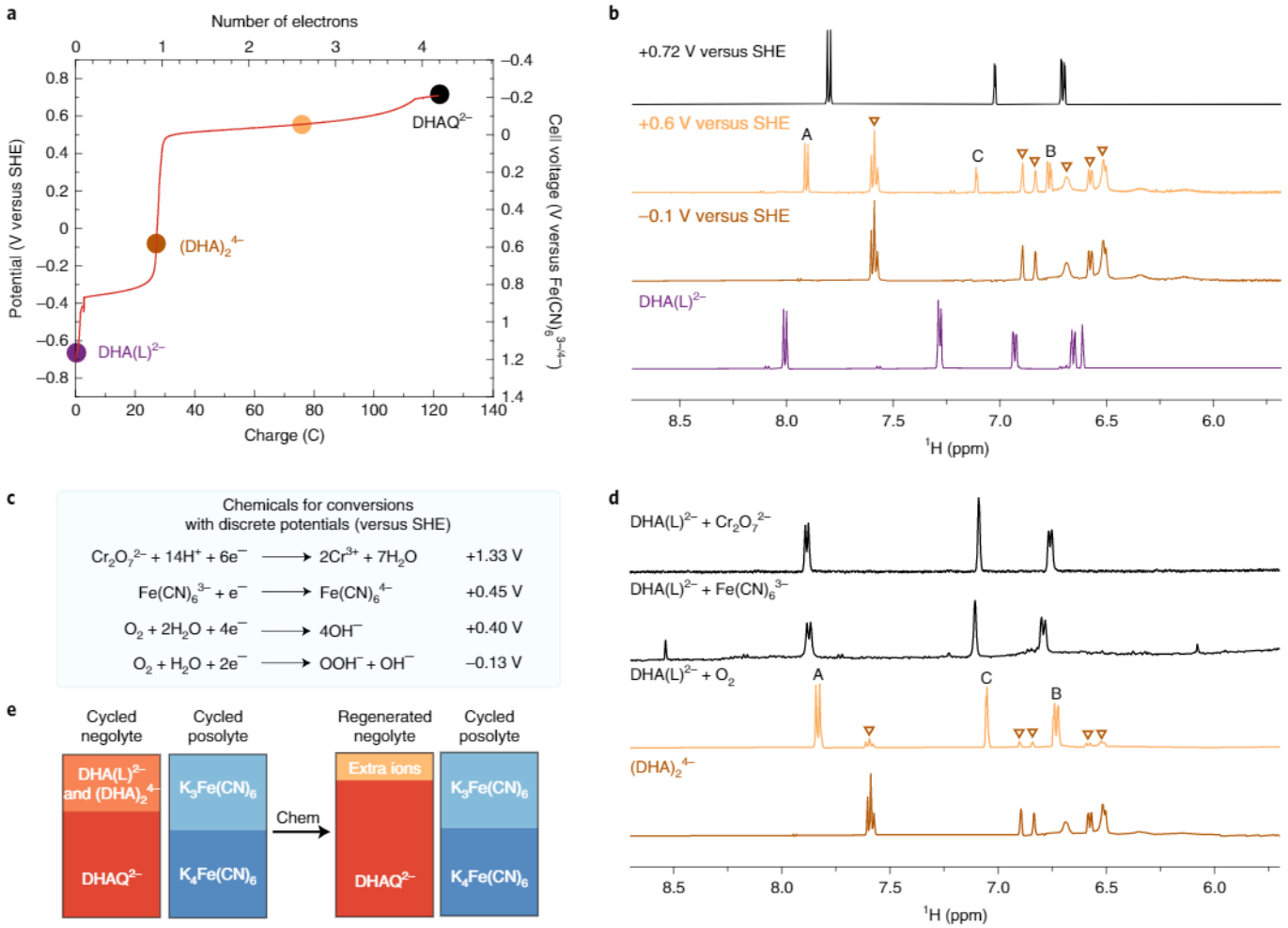

Fig. 3 | Electrochemical versus chemical oxidations of DHA(L)$^{2-}$. **a**, Voltage profile of the DHA(L)$^{2-}$|[Fe(CN)$_6$]$^{3-/4-}$ flow cell with an embedded Hg/HgO (1 M KOH) reference electrode. **b**, Ex situ ^{1}H NMR spectra acquired at different potentials of DHA(L)$^{2-}$ negolytes taken from the DHA(L)$^{2-}$|Fe(CN)$_6$ flow cell. The battery is composed of 6 ml, 50 mM DHA(L)$^{2-}$ in the negolyte and a mixture of 120 ml, 40 mM K_4[Fe(CN)$_6$] and 20 mM K_3[Fe(CN)$_6$] in the posolyte. A galvanostatic discharge was performed at −40 mA cm^{-2} with a potential hold at −0.2 V versus Fe(CN)$_6$ with a current cutoff of −1 mA cm^{-2}. The solid circles in **a** indicate the points at which aliquots were extracted for ex situ analysis. Bottom to top: the aliquot taken from the DHA(L)$^{2-}$ negolyte before any potential is applied (purple), and an aliquot is taken when the potential of the negolyte was at −0.1 V (brown), +0.5 V (yellow) and +0.65 V (black). The hollow brown triangles correspond to (DHA)$_2^{4-}$ peaks. A, B and C indicate the DHAQ^{2-} resonances as shown in Fig. 1c. **c**, Chemicals used for DHA(L) oxidation and their reduction potentials. **d**, ^{1}H NMR spectra of (DHA)$_2^{4-}$ and aliquots (0.1 M, 100 µl each) taken after the different chemical reactions. Bottom to top: aliquot from (DHA)$_2^{4-}$, which serves as a control (brown). Aliquots from DHA(L)$^{2-}$ samples exposed to oxygen (yellow), mixed with five equivalents of ferricyanide (black) (the peak at 8.52 ppm corresponds to the partially protonated hydroxyl groups in DHAQ), and mixed with five equivalents of $K_2Cr_2O_7$ in acid (black), the suspension being filtered to collect the organic precipitates and remove the $Cr^{3+/6+}$ solution, the precipitates then being redissolved in base. Relevant overall chemical reactions include: $O_2 + 4DHA(L)^{2-} \rightarrow 2(DHA)_2^{4-} + 2H_2O$, $O_2 + OH^- + 2DHA(L)^{2-} \rightarrow (DHA)_2^{4-} + OOH^- + H_2O$, and $O_2 + DHA(L)^{2-} \rightarrow DHAQ^{2-} + H_2O$; $DHA(L)^{2-} + 4Fe(CN)_6^{3-} + 4OH^- \rightarrow DHAQ^{2-} + 4Fe(CN)_6^{4-} + 3H_2O$; $2Cr_2O_7^{2-} + 16H^+ + 3DHA(L) \rightarrow 4Cr^{3+} + 11H_2O + 3DHAQ$. Note that in acidic conditions, DHA(L)$^{2-}$ and DHAQ^{2-} are protonated and thus become neutral molecules. **e**, Schematic of the rejuvenated DHAQ^{2-} flow cell that results from chemical regeneration. Extra ions such as Cr^{3+}, $Fe(CN)_6^{4-}$ or OH^- will be inevitably introduced to the negolyte due to the use of chemicals for conversion. The small variation of DHAQ^{2-} chemical shifts among different samples is due to the slight differences in pH.

peaks from (DHA)$_2^{4-}$ dominate at −0.1 V; the peaks from (DHA)$_2^{4-}$ and DHAQ^{2-} coexist at 0.5 V; eventually, the peaks from DHAQ^{2-} dominate at 0.65 V. These potential-driven stepwise conversions corroborate the in situ ^{1}H NMR results (Fig. 1d,e), indicating that electrochemical oxidation is indeed feasible. It is worth noting that the chemical shifts of the molecules between the in situ and ex situ NMR spectra are different, which is ascribed to the difference in concentration of hydroxide ions[12] and organic molecules[19]. This is a consequence of our different NMR sample preparation methods: for the in situ NMR tests, we used 0.1 M DHAQ, 1 M KOH in D_2O as the negolyte and tracked the NMR spectra directly in real time; by contrast, for the ex situ NMR measurements, we first took aliquots comprising 100 µl of 0.1 M DHAQ, 1 M KOH in H_2O and then diluted them with 550 µl of D_2O for the NMR measurements.

Although chemical oxidation of DHA(L)$^{2-}$ by O_2 recovers a substantial amount of DHAQ^{2-}, some (DHA)$_2^{4-}$ remains due to the proximity of the dimer (0.57 V versus SHE; see Extended Data Fig. 1b) and oxygen redox potentials (0.40 V versus SHE) (Fig. 3c). By contrast, other chemical oxidants with higher oxidation potentials such as $Cr_2O_7^{2-}$ under acidic conditions (Fig. 3d) or ferricyanide under basic conditions, fully convert DHA(L)$^{2-}$ into DHAQ^{2-} (Supplementary Fig. 5). However, they inevitably introduce extra

ions into the electrolyte, leading to system imbalance. By contrast, as illustrated in Fig. 3 and in other experiments involving pure $DHA(L)^{2-}$ (Extended Data Fig. 1), the results shown here clearly demonstrate that conversion of $DHA(L)^{2-}$ and $(DHA)_2^{4-}$ back to $DHAQ^{2-}$ is also possible by electrochemical oxidation. Electrolyte regeneration by electrochemical oxidation has several advantages over chemical oxidation. First, the disproportionation reaction, which creates $DHA(L)^{2-}$, formally involves two coupled reactions: (1) oxidation to form $DHAQ^{2-}$ and (2) reduction via the hydrogenation of $DHAQ^{4-}$ by water and generation of hydroxide ions, which, together, unbalance the SOC and change the pH of the electrolytes. Electrochemical regeneration of $DHAQ^{2-}$ from $DHA(L)^{2-}$ rebalances the SOC and restores the pH, closing the cycle and bringing the cell back to its initial conditions (Fig. 2c). By contrast, chemical oxidation of $DHA(L)^{2-}$ further alters the chemical composition and pH of the electrolyte solution (Fig. 3c,e). Second, electrochemical regeneration avoids the costs associated with periodically adding chemical oxidants to the negolyte. Third, electrochemical regeneration does not add solute to the negolyte that might eventually cause precipitation of active species or cross the membrane and interact deleteriously with posolyte species. Fourth, the majority of the electrochemical oxidation occurs at a positive, albeit lower cell potential in the discharge direction and thus consists of usable energy, which in turn increases the overall energy efficiency of the battery.

Electrochemical regeneration of DHAQ|$Fe(CN)_6$ flow battery. To demonstrate the effectiveness and sustainability of the electrochemical regeneration strategy, a $DHAQ^{2-}$|$[Fe(CN)_6]^{3-/4-}$ full cell was cycled with an additional discharge step down to −0.1 V every 50 cycles (Fig. 4). During each of these additional discharge treatments (Fig. 4c), the potentials of both the negolyte and the full cell contain two additional oxidation plateaus, which correspond to the dimerization of $DHA(L)^{2-}$ and the subsequent oxidation of the $(DHA)_2^{4-}$ back to $DHAQ^{2-}$ (Fig. 3a). The capacity measured during the first oxidation plateau (at around −0.3 V versus SHE) is almost one-third the capacity measured during the second plateau (at around 0.6 V versus SHE). This observation, further confirmed by volumetrically unbalanced but compositionally symmetric cell testing (Supplementary Fig. 6), is consistent with the electrochemical oxidation of $DHA(L)^{2-}$ in Fig. 3a and the proposed reactions in Fig. 2a, as the oxidation of $DHA(L)^{2-}$ involves one electron whereas the dimer loses three electrons per molecule of $DHA(L)^{2-}$ to form $DHAQ^{2-}$. Figure 4a,b shows substantial recovery after each of these treatments, in agreement with the evidence from in situ NMR of decomposition and recovery under similar conditions (Fig. 1a,b). In all cases, the ratio of capacity recovery to capacity lost in the preceding 50 cycles always exceeds 93% except for the first case (71%), and averages to 94.7%. Repeated experiments show similar behaviour with unusually high recovery following a segment with a low recovery ratio (Extended Data Fig. 2), which suggests that any unconverted $DHA(L)^{2-}$ remains in the electrolyte for subsequent regeneration. Although extra electrical energy would be required to reverse the polarity (Extended Data Fig. 3), the energetic cost for 13 such regeneration processes in Fig. 4a only accounts for 0.025% of total discharged energy over 700 cycles (13 days), which is negligible. Hydroxide ions are expected to be oxidized to oxygen during the electrochemical regeneration, the generated oxygen will be reduced by $DHAQ^{4-}$ to hydroxide ions and return to the negolyte in a closed flow cell system, thus restoring the pH of electrolytes.

The average recovery in Fig. 4a leads to an overall residual fade rate of 0.38% per day, which is more than an order of magnitude improvement over the initial instantaneous fade rate in this experiment of 6.45% per day. Additional cell cycling experiments also suggest that the effectiveness of the regeneration treatment is unrelated to the amount of $DHA(L)^{2-}$ formed (Supplementary Fig. 7). This implies that the residual capacity fade of the battery is no longer related to the previously published anthrone-related capacity fade mechanism[12]. By addressing this degradation mechanism with electrochemical regeneration, it is no longer necessary to perform SOC-restricted cycling, thereby enabling more of the negolyte to be used, with a corresponding reduction in system cost. Although long-term cycling and recovery experiments such as the one shown in Fig. 4a have not demonstrated the complete recovery of battery capacity, extensive characterization of cycled negolytes with substantial capacity loss has not indicated the accumulation of any appreciable decomposition products after additional discharge at −0.1 V. Concentration measurements by cyclic voltammetry and NMR of the negolyte suggest that the concentration of $DHAQ^{2-}$ has not been lost (Extended Data Fig. 4). Although the unchanged concentration of $DHAQ^{2-}$ may be overestimated by water splitting in the negolyte and water cross-over from negolyte to posolyte during electrochemical oxidation, only the signal from DHAQ is detected by liquid chromatography–mass spectrometry (LC–MS), confirming that most of the DHAQ is maintained, and that the concentration of decomposition compounds—if they are produced over cycling—is below the instrument detection limit of LC–MS. We note that water splitting and cross-over lead to lower coulombic efficiency, capacity imbalance and pH fluctuation[20]. The data in this study take into account the possible capacity-limiting effect of the ferrocyanide posolyte by complete replacement of the posolyte (Supplementary Fig. 8), thereby leaving only two remaining hypotheses for this secondary fade mechanism: an apparent capacity fade due to the interaction of fixed cycling voltage limits with open circuit voltage drift in the electrolytes; or molecular decomposition mechanisms that have thus far been undetected, such as fragmentation, polymerization or $DHAQ^{2-}$ tautomerization[21]. Further investigation into these secondary capacity fade mechanisms is an important direction for future research. Note that, as in many laboratory-scale research studies, excessive $Fe(CN)_6^{3-/4-}$ was used in all full cell tests to minimize the influence of the posolyte side reaction[22] on negolyte capacity recovery. However, for practical implementation it is entirely feasible to start with a $DHAQ^{2-}$|$[Fe(CN)_6]^{4-}$ capacity-balanced cell, as all reactions in both electrolytes are electron balanced (Supplementary Fig. 9)[23].

To investigate the influence of concentration of DHAQ on the effectiveness of electrochemical regeneration strategy, as well as avoid reversing the polarity, we further built a 0.5 M DHAQ-based full cell and deep discharged it to 0.01 V from the 11th to 210th cycle (Fig. 4d). The 0.5 M $DHAQ^{2-}$|$[Fe(CN)_6]^{3-/4-}$ full cell shows lower instantaneous temporal fade rates of 2.89% and 2.74% per day in its first and last ten cycles, respectively, than its 0.1 M counterpart with normal cycling. The difference was caused by the difference in discharge voltage cutoffs (0.6 V versus 0.9 V). The voltage of 0.6 V used in 0.5 M $DHAQ^{2-}$ cell was low enough to electrochemically oxidize the accumulated DHA(L) to redox-active[12] $(DHA)_2$, which then contributed to the accessible capacity, affording lower instantaneous temporal fade rates. Given that the reduction potential of ferricyanide to ferrocyanide is just above the oxidation potentials of $DHA(L)^{2-}$ and $(DHA)_2^{4-}$ to $DHAQ^{2-}$ (Fig. 3c and Extended Data Fig. 1b), and that ferricyanide barely oxizides $DHA(L)^{2-}$ to $DHAQ^{2-}$ (Fig. 3d and Supplementary Fig. 5), during the five-day period between the 11th and 210th cycle, we first discharged the cell to 0.9 V and then immediately deep discharged it to 0.01 V, leading to an average fade rate of 0.18% per day without reversing the polarity or requiring extra energetic cost. Note that $(DHA)_2^{4-}$ is not completely oxidized to $DHAQ^{2-}$ under these conditions (Supplementary Fig. 10), as complete conversion requires a more positive potential; $(DHA)_2^{4-}$ peaks have indeed been detected in ^{1}H NMR when discharged to 0 V under similar conditions (Extended Data Fig. 1f and Supplementary Fig. 10). Our interpretation of the slight capacity drop at the 210th cycle (Fig. 4d) is that the residual $(DHA)_2^{4-}$ is redox-active over the deep-discharge cycling[15], but no longer contributing capacity during the subsequent normal cycling.

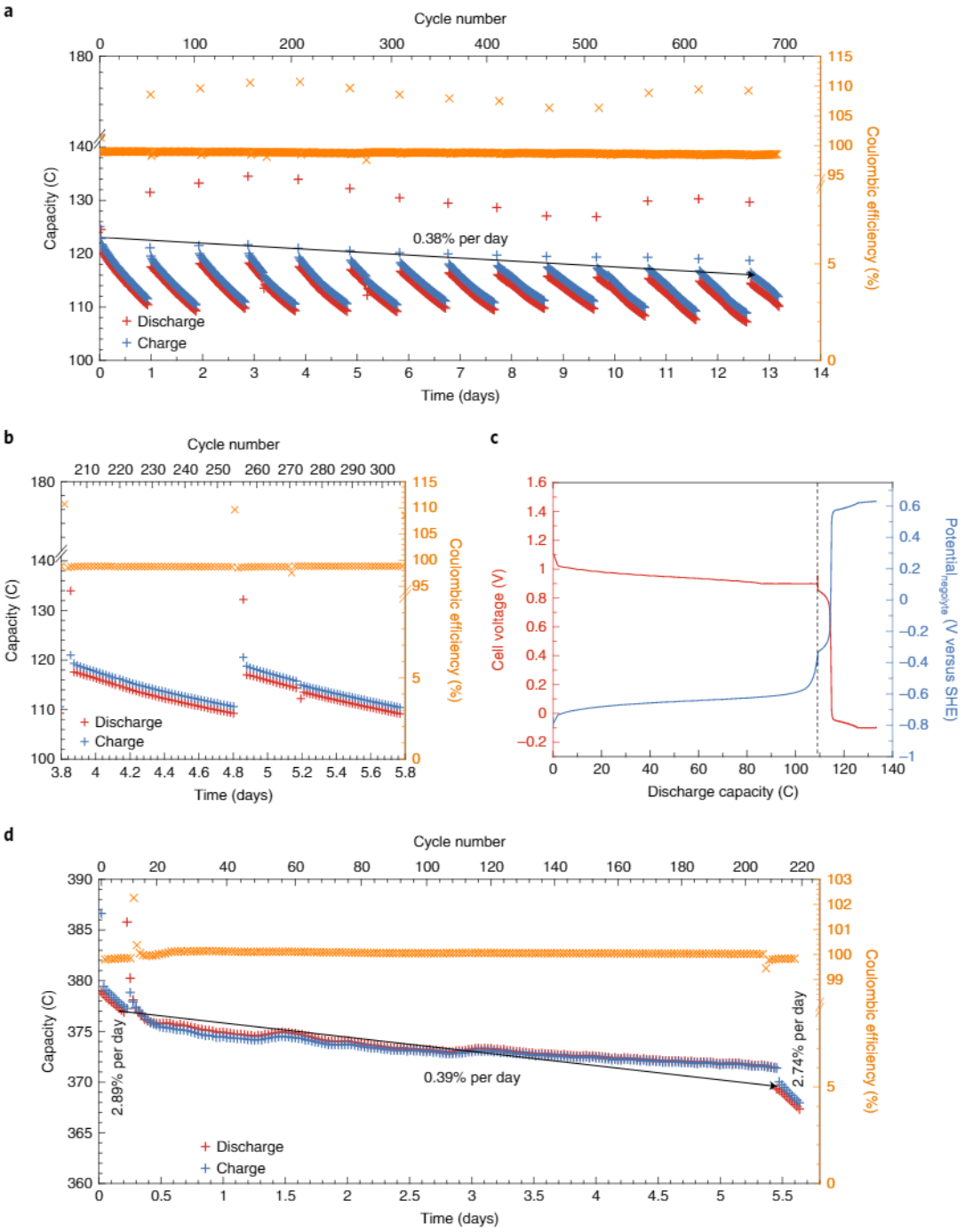

Fig. 4 | Long-term cycling of $DHAQ^{2-/4-}$|$[Fe(CN)_6]^{3-/4-}$ flow battery with capacity recovery by electrochemical regeneration of the negolyte. a, Repeated application of the electrochemical regeneration step of negolyte in a flow battery. **b**, A highlighted example of electrochemical regeneration of negolyte on day 4.8 during discharge. **c**, An example of the full cell and negolyte potential during the additional discharge step down to −0.1 V. The battery was composed of 6.5 ml, 100 mM $DHAQ^{2-}$, 1 M KOH in the negolyte, and a mixture of 35 ml, 60 mM $K_4[Fe(CN)_6]$ and 30 mM $K_3[Fe(CN)_6]$, 1 M KOH in the posolyte. Galvanostatic cycling at ±40 mA cm^{-2} was performed with potential holds at 0.9 and 1.4 V during normal cycles, with current cutoffs of −1 and 2 mA cm^{-2} for discharge and charge, respectively. Every 50 cycles there was an additional discharge step at −2 mA cm^{-2} until the potential reached −0.1 V, and a further hold until the current decreased to −0.4 mA cm^{-2}. The overall fade rate is 0.38% per day. Red and blue plus symbols represent discharge and charge capacity, respectively. Orange crosses represent coulombic efficiency. The cell voltage and potential changes during the standard cycling protocol in **c** are shown to the left of the dashed line, whereas to the right are those during the conversions of $DHA(L)^{2-}$ to $(DHA)_2^{4-}$, and of $(DHA)_2^{4-}$ to $DHAQ^{2-}$. **d**, High concentration DHAQ|$Fe(CN)_6$ flow cell with deep discharge (0.01 V) but no polarity reverse; 4 ml 0.5 M $DHAQ^{2-}$ in 1 M KOH in the negolyte and a 35 ml mixture of 0.35 M $K_4[Fe(CN)_6]$ and 0.05 M $K_3[Fe(CN)_6]$, 1 M KOH in the posolyte. Galvanostatic cycling at ±100 mA cm^{-2} with potential holds at 1.5 V and 0.6 V during normal cycles, that is, without the deep-discharge steps for the first and last ten cycles, with current cutoffs of ±2 mA cm^{-2} for charge and discharge. Galvanostatic cycling at ±100 mA cm^{-2} with potential holds at 1.5 V for charge and 0.9 V then 0.01 V for discharge during deep-discharge cycles (11th to 210th cycle) with current cutoffs of ±2 mA cm^{-2}. Flow cell cycling experiments for the low (**a**) and high (**d**) concentrations were each repeated independently three times with similar results.

The overall residual fade rate is thus 0.39% per day; this is expected to be futher reduced when deep discharge and periodic reverse polarity are combined.

The high fade rate of $DHAQ^{2-/4-}$ makes it particularly suitable for demonstrating the effectiveness of the electrochemical regeneration method described in this study; however this method would also be applicable to other anthraquinone negolytes with low (0.02–0.1% per day) or moderate (0.1–1% per day) fade rates[3], which also suffer from the same anthrone disproportionation mechanism. One such example is anthraquinone-2,7-disulfonic acid (AQDS)[11,24], which has a much lower fade rate of 0.1% per day in acid at room temperature[25], but decomposes to anthrone (anthranol)-2,7-disulfonic acid (ADS) over cycling (Supplementary Fig. 11)[26]. Our preliminary results confirm that ADS (both pure ADS and that produced by cycling AQDS) can be chemically and electrochemically converted to AQDS (Supplementary Figs. 12–14). This approach should therefore reduce the overall fade rate of these negolytes, potentially enabling them to reach electrolyte lifetimes comparable with more recent studies that use more complex and costly reactants[5–7]. More generally, we expect the same anthrone-based capacity fade mechanism to be present in even those ultra-long-lifetime anthraquinone electrolytes and, as such, could also be reversed by the electrochemical regeneration method demonstrated in this work. More broadly, many of the published potentially inexpensive molecules demonstrate fade rates ranging from 0.1% to 1% per day[3]. If the same improvement can be achieved for other molecules, we would expect to reduce their temporal fade rates to 0.005–0.05% per day, which would render them practically useful. This may permit them to satisfy the lifetime to cost technoeconomic targets elaborated in ref. [27].

Conclusion

This work demonstrates the power of in situ ^{1}H NMR and EPR metrologies to reveal and quantify the degradation reactions occurring in electrochemical flow cells and ultimately use this insight to regenerate the redox-active molecules. Specifically, we have shown that the decomposition compounds $DHA(L)^{2-}$ that form in cycled DHAQ electrolytes can be converted electrochemically back to $DHAQ^{2-}$, validating our proposed degradation and regeneration mechanisms. A mechanistic study indicates that the conversion proceeds in two steps: first, $DHA(L)^{2-}$ is oxidized to $(DHA)_2^{4-}$ with one-electron transfer at –0.32 V versus SHE; second, $(DHA)_2^{4-}$ is oxidized to $DHAQ^{2-}$ with three-electron transfer at +0.57 V versus SHE, with the two steps consuming one and three hydroxide ions, respectively. These oxidative interventions close the loop comprising DHAQ-related potential-driven molecular conversions. We then demonstrate the repeated electrochemical regeneration of the DHAQ|$Fe(CN)_6$ alkaline flow battery. Electrochemical regeneration not only rejuvenates the negolyte, but also rebalances the state of charge of both electrolytes. AQDS preliminary studies further show both the feasibility of electrochemical regeneration at pH 0 and that this is not a peculiar feature of DHAQ. The electrochemical regeneration method can be extended to other anthraquinones susceptible to anthrone formation and we expect that similar strategies may also be applicable for other redox-active organic molecules. Electrochemical regeneration could permit redox-active organic molecules to reach the required combination of performance, cost and lifetimes necessary for aqueous organic redox flow batteries to become attractive solutions for the storage of intermittent renewable electricity.

Online content

Any methods, additional references, Nature Research reporting summaries, source data, extended data, supplementary information, acknowledgements, peer review information; details of author contributions and competing interests; and statements of data and code availability are available at https://doi.org/10.1038/s41557-022-00967-4.

Received: 16 December 2021; Accepted: 4 May 2022;
Published online: 16 June 2022

References

1. Huskinson, B. T. et al. A metal-free organic–inorganic aqueous flow battery. *Nature* **505**, 195–198 (2014).
2. Lin, K. et al. Alkaline quinone flow battery. *Science* **349**, 1529–1532 (2015).
3. Kwabi, D. G., Ji, Y. & Aziz, M. J. Electrolyte lifetime in aqueous organic redox flow batteries: a critical review. *Chem. Rev.* **120**, 6467 (2020).
4. Beh, E. S. et al. A neutral pH aqueous organic–organometallic redox flow battery with extremely high capacity retention. *ACS Energy Lett.* **2**, 639–644 (2017).
5. Kwabi, D. G. et al. Alkaline quinone flow battery with long lifetime at pH 12. *Joule* **2**, 1894–1906 (2018).
6. Ji, Y. et al. A phosphonate-functionalized quinone redox flow battery at near-neutral pH with record capacity retention rate. *Adv. Energy Mater.* **9**, 1900039 (2019).
7. Wu, M. et al. Extremely stable anthraquinone negolytes synthesized from common precursors. *Chem* **6**, 1432–1442 (2020).
8. Jin, S. et al. Near neutral pH redox flow battery with low permeability and long-lifetime phosphonated viologen active species. *Adv. Energy Mater.* **10**, 2000100 (2020).
9. Pang, S., Wang, X., Wang, P. & Ji, Y. Biomimetic amino acid functionalized phenazine flow batteries with long lifetime at near-neutral pH. *Angew. Chem. Int. Ed.* **60**, 5289 (2021).
10. Xu, J., Pang, S., Wang, X., Wang, P. & Ji, Y. Ultrastable aqueous phenazine flow batteries with high capacity operated at elevated temperatures. *Joule* **5**, 2437–2449 (2021).
11. Gregory, T. D., Perry, M. L. & Albertus, P. Cost and price projections of synthetic active materials for redox flow batteries. *J. Power Sources* **499**, 229965 (2021).
12. Goulet, M.-A. et al. Extending the lifetime of organic flow batteries via redox state management. *J. Am. Chem. Soc.* **141**, 8014–8019 (2019).
13. Zhao, E. W. et al. In situ NMR metrology reveals reaction mechanisms in redox flow batteries. *Nature* **579**, 224–228 (2020).
14. Zhao, E. W. et al. Coupled In situ NMR and EPR studies reveal the electron transfer rate and electrolyte decomposition in redox flow batteries. *J. Am. Chem. Soc.* **143**, 1885–1895 (2021).
15. Jing, Y. et al. In situ electrosynthesis of anthraquinone electrolytes in aqueous flow batteries. *Green Chem.* **22**, 6084–6092 (2020).
16. Goulet, M. A. et al. Correction to "Extending the lifetime of organic flow batteries via redox state management." *J. Am. Chem. Soc.* **143**, 14019 (2021).
17. McCann, G. M., McDonnell, C. M., Magris, L. & O'Ferrall, R. A. M. Enol–keto tautomerism of 9-anthrol and hydrolysis of its methyl ether. *J. Chem. Soc.* **2**, 784–795 (2002).
18. Zhao, E. W., Shellard, E. J. K., Klusener, P. A. A. & Grey, C. P. In situ bulk magnetization measurements reveal the state of charge of redox flow batteries. *Chem. Commun.* **58**, 1342–1345 (2022).
19. Mitra, A., Seaton, P. J., Assarpour, R. A. & Williamson, T. Unprecedented concentration dependent chemical shift variation in ^{1}H-NMR studies: a caveat in the investigations of molecular recognition and structure elucidation. *Tetrahedron* **54**, 15489 (1998).
20. Yao, Y., Lei, J., Shi, Y., Ai, F. & Lu, Y.-C. Assessment methods and performance metrics for redox flow batteries. *Nat. Energy* **6**, 582–588 (2021).
21. Fain, V. Y., Zaitsev, B. E. & Ryabov, M. A. Anthraquinones tautomerism: VII. Hydroxy-substituted anthraquinones. *Russ. J. Org. Chem.* **43**, 1460 (2007).
22. Páez, T., Martínez-Cuezva, A., Palma, J. & Ventosa, E. Revisiting the cycling stability of ferrocyanide in alkaline media for redox flow batteries. *J. Power Sources* **471**, 228453 (2020).
23. Páez, T., Martínez-Cuezva, A., Marcilla, R., Palma, J. & Ventosa, E. Mitigating capacity fading in aqueous organic redox flow batteries through a simple electrochemical charge balancing protocol. *J. Power Sources* **512**, 230516 (2021).
24. Dieterich, V. et al. Estimating the cost of organic battery active materials: a case study on anthraquinone disulfonic acid. *Translational Mater. Res.* **5**, 034001 (2018).
25. Goulet, M.-A. & Aziz, M. J. Flow battery molecular reactant stability determined by symmetric cell cycling methods. *J. Electrochem. Soc.* **165**, A1466 (2018).
26. Wang, F. et al. Stable tetrasubstituted quinone redox reservoir for enhancing decoupled hydrogen and oxygen evolution. *ACS Energy Lett.* **6**, 1533–1539 (2021).
27. Brushett, F. R., Aziz, M. J. & Rodby, K. E. On lifetime and cost of redox-active organics for aqueous flow batteries. *ACS Energy Lett.* **5**, 879–884 (2020).

Publisher's note Springer Nature remains neutral with regard to jurisdictional claims in published maps and institutional affiliations.

© The Author(s), under exclusive licence to Springer Nature Limited 2022

Methods

In situ NMR and EPR study. *Flow cell assembly.* The cell assembly was described in detail in our previous work[13]. Briefly, graphite flow plates with serpentine flow patterns were used for both electrodes. Each electrode is composed of 4.6 mm carbon felt (SIGRACELL®) with a 5 cm^2 active area, which was used without further treatment. Nafion 117 was used as the ion transport membrane. Pretreatment of the Nafion 117 membrane was performed by first heating the membrane in 80 °C deionized water for 20 min and then soaking it in 5% hydrogen peroxide solution for 35 min. The flow rate was set at 13.6 ml min^{-1}.

Electrochemical cycling. The cell (Supplementary Fig. 1a,b) was charged by a constant current of 30 mA cm^{-2}, followed by a voltage hold at 1.7 V for 42 h. It was then discharged by a constant current of −30 mA cm^{-2}, followed by a voltage hold at 0.5 V for 7.4 h, at 0.2 V for 1 h and −0.1 for 0.6 h. After the voltage hold, the battery was set in a rest state for 36.8 h.

Following the rest period, the voltage was decreased from 0.1 V to −0.3 V in steps of 0.1 V, holding for 2 h at each voltage step. Then the battery was charged by a constant current of 20 mA cm^{-2} followed by a voltage hold at 1.7 V for 1 h, discharged by a constant current of −20 mA cm^{-2} followed by a voltage hold at 0.6 V for 1 h. The charge–discharge cycles were repeated three times.

The volumetric loss of electrolyte solution was measured by marking the liquid level in the electrolyte reservoir (a glass cylindrical tube with inlet and outlet) before the cycling and marking the liquid level after the cycling. The volume difference between these two marks were measured, and is equal to the volumetric loss.

Online NMR and EPR set-up. The set-up has been described in detail in ref. [12]. Briefly, it consists of a flow cell system, a bench-top EPR (MS5000, Magnettech) and an NMR (300 MHz, Bruker) spectrometer. The electrolyte solution is pumped through the flow cell and then flowed through the EPR and NMR magnets, and finally back to the electrolyte reservoir. The direction of flow is from the bottom to the top through both magnets. 1.588 mm OD and 1.016 mm ID perfluoroalkoxy alkane tubes are used to connect the electrolyte reservoir, the battery, and the EPR and NMR sampling tubes. A flow-through NMR sampling tube with an OD of 10 mm was used. A flat EPR cell (E4503, Magnettech) was used to minimize heating of the aqueous solution by microwave irradiation. The cell is orientated in the resonator such that the strength of the magnetic field is maximized, and the strength of the electric field is minimized across the sample. The time it takes for a round-trip from and back to the electrolyte reservoir is 64 s at a flow rate of 13.6 cm^3 min^{-1}. It takes 3 s for the electrolyte solution to travel from the electrolyte reservoir to the battery, 3 s from the battery to the EPR detection region, 29 s from the EPR to the NMR detection region, and 29 s from the NMR detection regions back to the electrolyte reservoir. Data reported in Supplementary Fig. 3 were acquired by the coupled online NMR and EPR method. As no EPR-active degradation products were detected, the rest of the in situ data were acquired by online NMR only.

Pseudo-2D NMR. Pseudo-2D NMR experiments were performed on flowing electrolyte solution by direct excitation with a 90° radiofrequency pulse. Each NMR spectrum is acquired by collecting eight free induction decays with a recycle delay of 10 s. The pulse width for a 90° pulse was 29 µs at 60 W. All spectra were referenced to the water chemical shift at 4.79 ppm before cell cycling starts.

For the DHAQ concentration calculations, the pseudo-2D NMR spectra were first baseline-corrected by a fourth-order polynomial function. The resonance of DHAQ proton A was used for the calculation of DHAQ concentration. The signal integral of resonance A before the start of electrochemical cycling is normalized to 100 mM. The signal-to-noise ratio for resonance A at 100 mM is 696.7. A signal-to-noise ratio of 3 sets the detection limit; the detection limit for the in situ NMR using the current parameters is therefore 0.4 mM.

2D COSY NMR. Two-dimensional homonuclear COSY NMR experiments were performed on the electrolyte solution with $DHA(L)^{2-}$ during flow and on the electrolyte solution with $(DHA)_2^{4-}$ when the flow is stopped. Pulsed field gradient-enhanced double quantum filter COSY pulse sequences were applied[28]. For the $DHA(L)^{2-}$ spectrum acquired (Supplementary Fig. 2c), the second dimension was constructed using 512 increments spanning 10 ppm. The recycle delay was 2 s and the number of scans for each increment was 4. For the spectrum acquired on $(DHA)_2^{4-}$ (Supplementary Fig. 2d), the second dimension was constructed using 1,024 increments spanning 10 ppm. The recycle delay was 2 s and the number of scans for each increment was 16.

EPR parameters. For the EPR experiments, the magnetic field was swept from 336.5 to 339 mT; the microwave power P was 0.5 mW and the modulation amplitude B_m was 0.001 mT. The acquisition time per EPR spectrum is 88 s, with a scanning time of 60 s, a coupling time of 20 s (time for automatic tuning) and a delay time of 8 s.

Electrochemical characterizations. *Cyclic voltammetry measurements.* A 5 mm diameter glassy carbon working electrode was used for all three-electrode cyclic voltammetry tests, with a Ag/AgCl reference electrode (BASi, pre-soaked in 3 M NaCl solution) and a graphite counter electrode. All cyclic voltammetry, linear sweep voltammetry and chronoamperometry measurements were conducted on Gamry Instruments and CHI Instrument electrochemical analysers.

Flow cell set-up. Flow cell experiments were constructed with cell hardware from Fuel Cell Tech or in-house cell with end plates made from PVC. Both designs were assembled into a zero-gap flow cell configuration using either pyrosealed POCO graphite flow plates or resin-impregnated carbon flow plates from MWI with identical interdigitated flow fields. Each electrode comprised one or two layers of Zoltek PXFB carbon cloth with a geometric surface area of 5 cm^2. Nafion 117 membranes pre-soaked in 1 M KOH for at least 24 h were used in all cell cycling tests.

To independently track the potential of the negative electrode as presented in Fig. 3, a Hg/HgO reference electrode (BASi, with an internal electrolyte of 1 M KOH) was positioned externally on the inlet of the negolyte stream.

Materials synthesis. DHA(L) was synthesized as described in ref. [12]. In brief, DHAQ and excess stannous chloride were refluxed for 7 h in concentrated HCL. The resulting solution was cooled to room temperature, and the precipitate was collected by vaccum filtration. The collected solid was washed with deionized water then dried in vacuo to afford a pale yellow powder.

Anthrone-2,7-disulfonic acid was synthesized by following the similar procedure. Anthraquinone-2,7-disulfonate sodium (4.12 g, 10.0 mmol) and excess stannous chloride (9.50 g, 50.0 mmol) in 1 M hydrochloric acid aqueous solution were heated at 80 °C for 24 h. The resulting solution was cooled to room temperature, and the precipitate was collected by vacuum filtration. The solid was dried in vacuo to afford a pale yellow powder. Under nitrogen protection, the powder was then dissolved in 1 M HCl and subject to ion-exchange column to obtain ADS, the solution was condensed by rotavap and dried in vacuo to afford the product (90%).

Anthraquinone-2,7-disulfonate sodium was purchased from ASTATech and ion exchanged to anthraquinone-2,7-disulfonic acid.

Characterization. Ex situ ^1H NMR spectra were recorded on Varian INOVA 500 spectrometers at 500 MHz. Aliquots were taken and put in D_2O, corresponding NMR spectra were recorded in D_2O with the residual H_2O (δ4.79 ppm for ^1H NMR). LC–MS was conducted on a Bruker microTOF-QII mass spectrometer. The sample was diluted by water/acetonitrile (V/V = 1:1) to the desired concentration (~20 µM) before LC–MS measurements.

Data availability

Data in the main paper and its Supplementary Information are available from https://doi.org/10.6084/m9.figshare.19612128. Source Data are provided with this paper.

References

28. Shaw, A. A. S., Christophe, Dauphin, Jean-Francois & Ancian, Bernard Artifact-free PFG-enhanced double-quantum-filtered COSY experiments. *J. Magn. Reson. A* **120**, 110–115 (1996).

Acknowledgements

Research at Harvard was supported by the US National Science Foundation through grant no. CBET-1914543, by a US DOE award no. DE-AC05-76RL01830 through PNNL subcontract no. 535264, and by a grant from the Massachusetts Clean Energy Center. Research at University of Cambridge was supported by Centre of Advanced Materials for Integrated Energy Systems (CAM-IES), via EPSRC grant no. EP/P007767/1 and Shell. E.W.Z acknowledges the STFC Futures Early Career Award, grant no. ST/R006873/1. The funders had no role in study design, data collection and analysis, decision to publish or preparation of the manuscript. We acknowledge P.A.A. Klusener from Shell for useful discussions. We thank D. A. Pollack, and K. Amini for useful discussions.

Author contributions

M.J.A., R.G.G., C.P.G. supervised the project. Y.J., E.W.Z., M.-A.G., M.J.A., R.G.G. and C.P.G. conceived the idea. Y.J., E.W.Z. and M.-A.G. designed the experiment. E.W.Z. performed the in situ NMR and EPR experiments and analysis. Y.J. performed the ex situ NMR experiments and analysis. M.-A.G., M.B., E.M.F. and Y.J. performed DHA(L), ADS elctrochemical oxidation, and DHAQ and AQDS cell cycling. M.B. performed three-electrode cell tests. M.-A.G., S.J. and Y.J. performed postmortem CV, NMR, LC-NMR experiments and a cell cycling. M.B. performed t-cell cycling with periodic aeration. E.J. made intellectual contributions. M.W. and Y.J. synthesized DHA(L) and ADS, respectively. All authors contributed to the discussion of the project. Y.J., E.W.Z, M.-A.G., M.J.A., C.P.G. wrote the manuscript with input from all co-authors.

Competing interests

The authors declare no competing interests.

Additional information

Extended data is available for this paper at https://doi.org/10.1038/s41557-022-00967-4.

Supplementary information The online version contains supplementary material available at https://doi.org/10.1038/s41557-022-00967-4.

Correspondence and requests for materials should be addressed to Clare P. Grey, Roy G. Gordon or Michael J. Aziz.

Peer review information *Nature Chemistry* thanks Antoni Forner-Cuenca, Yi-Chun Lu and Edgar Ventosa for their contribution to the peer review of this work.

Reprints and permissions information is available at www.nature.com/reprints.

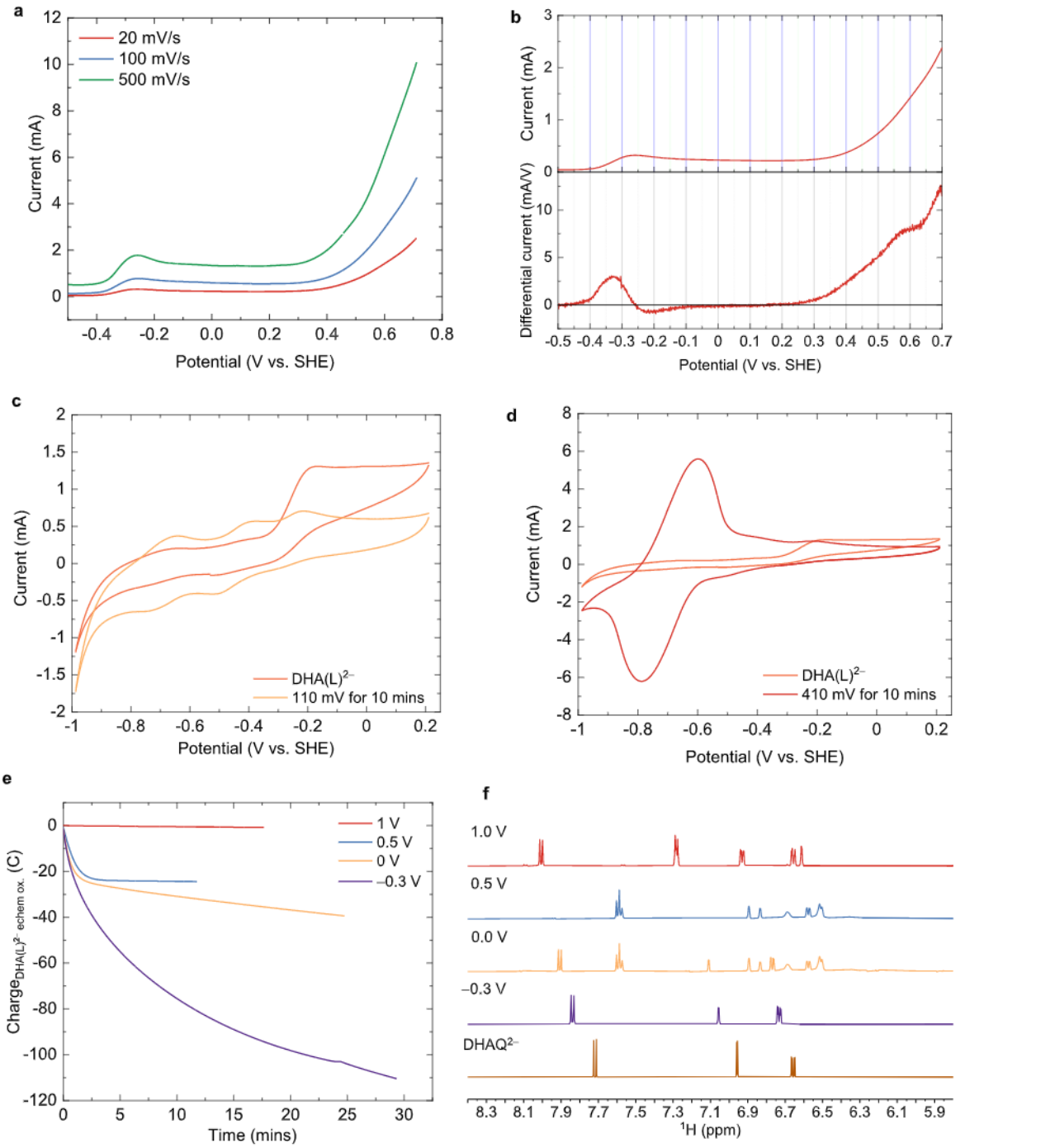

Extended Data Fig. 1 | Electrochemical oxidation of $DHA(L)^{2-}$. a & b, Linear sweep voltammetry (LSV) and the 1st order differential of 10 mM $DHA(L)^{2-}$ in 1 M KOH supporting electrolyte indicating a peak for dimerization reaction around −260 mV vs. SHE and a second oxidation reaction starting around +300 mV vs. SHE, before being overshadowed by oxygen evolution at around +650 mV vs. SHE. We consider the potentials (−0.32 V, + 0.57 V) at the 1st order differential peak current as the approximations of oxidation potentials of [$DHA(L)^{2-}$ to $(DHA)_2^{4-}$] and [$(DHA)_2^{4-}$ to $DHAQ^{2-}$]. The 1st order differential was from the LSV curve obtained at 20 mV/s. **c & d**, Cyclic voltammograms of 10 mM pure DHA in 1 M KOH before and after a + 110 mV vs. SHE 10-minute potential hold with a highly porous Zoltek PXFB working electrode. New peaks match those of dimer observed in a previous study[21]; cyclic voltammograms of 10 mM pure DHA in 1 M KOH before and after +410 mV vs. SHE 10-minute potential hold with a highly porous working electrode. New peaks match those of $DHAQ^{2-}$. **e**, Potential hold of 0.1 M $DHA(L)^{2-}$ in 1.2 M KOH negolyte in full cell containing a 2X excess of 50 mM $K_4[Fe(CN)_6]$ and 50 mM $K_3[Fe(CN)_6]$ posolyte. The Y-axis represent the number of coulombs extracted from $DHA(L)^{2-}$ electrolyte over electrochemical oxidation. **f**, ^1H NMR spectra of $DHA(L)^{2-}$ negolyte before and after 30-min hold at different cell voltages.

a

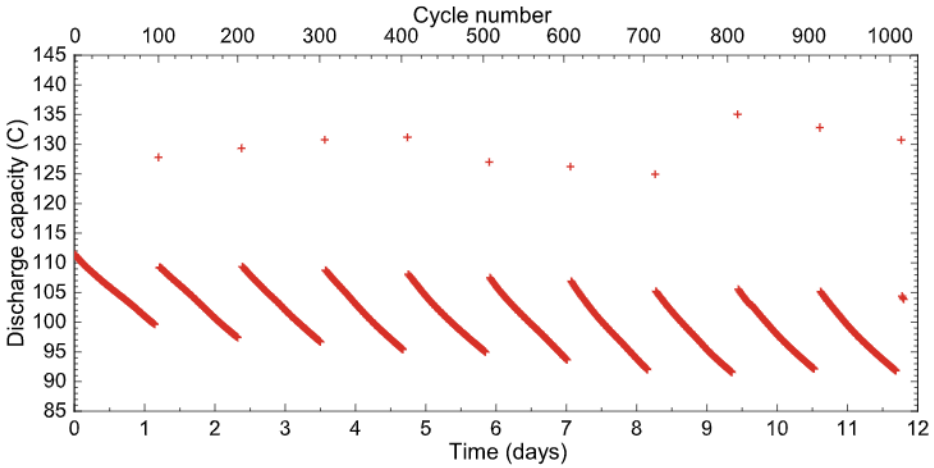

b

Channel	Potential (V)	Start Cap (C)	Finish Cap (C)	Lost (C)	Lost (%)	Restart Cap (C)	Recovered (C)	Recovered (%)
Ch01	-0.020	111.5	101.0	10.5	9.4	110.5	9.5	90.5
	0.020	110.5	99.7	10.8	9.8	109.7	10.0	92.6
	0.000	109.7	98.9	10.8	9.8	109.3	10.4	96.3
	0.000	109.3	97.7	11.6	10.6	108.7	11.0	94.8
	-0.020	108.7	98.0	10.7	9.8	108.4	10.4	97.2
	0.050	108.4	97.0	11.4	10.5	107.9	10.9	95.6
	0.100	107.9	95.9	12.1	11.2	107.4	11.5	95.4
	0.000	107.4	96.4	11.0	10.2	107.1	10.7	97.3
	0.000	107.1	96.3	10.8	10.0	106.7	10.4	96.7
Ch02	0.000	111.2	97.1	14.1	12.7	109.7	12.6	89.4
	-0.020	109.7	95.6	14.1	12.9	109.1	13.5	95.7
	0.020	109.1	94.6	14.5	13.3	108.5	13.9	95.9
	0.020	108.5	93.7	14.8	13.6	108.0	14.3	96.6
	0.000	108.0	93.9	14.1	13.1	107.5	13.6	96.5
	0.050	107.5	92.1	15.4	14.3	106.9	14.8	96.1
	0.100	106.9	91.9	15.0	14.0	101.8	9.8	65.7
	0.000	101.8	89.5	12.3	12.0	105.4	15.9	129.8
Ch03	0.020	111.4	99.6	11.8	10.6	109.3	9.7	82.2
	0.000	109.3	97.4	11.9	10.9	109.3	11.9	100.0
	-0.020	109.3	96.7	12.6	11.5	108.7	12.0	95.2
	-0.020	108.7	95.4	13.3	12.2	108.0	12.6	94.7
	0.020	108.0	95.0	13.0	12.0	107.5	12.5	96.2
	0.050	107.5	93.7	13.8	12.8	106.9	13.2	95.7
	0.100	106.9	92.0	14.9	13.9	105.2	13.2	88.6
	0.000	105.2	91.6	13.6	13.0	105.6	14.0	102.6
	0.000	105.6	92.1	13.5	12.7	105.2	13.1	97.1

Extended Data Fig. 2 | DHAQ regeneration hysteresis. a, Repeated application of electrochemical regeneration of negolyte in battery composed of 6 mL 100 mM $DHAQ^{2-}$ in the negolyte and a mixture of 35 mL 100 mM $K_4[Fe(CN)_6]$ and 50 mM $K_3[Fe(CN)_6]$ in the posolyte. Galvanostatic cycling at ±50 mA/cm² with potential holds at 1.0 and 1.5 V and current cutoff of ±1 mA/cm² during normal cycles. Every 50 cycles an additional discharge step at −2 mA/cm² until potential limit and a further hold until current decreases to −0.2 mA/cm². **b**, Aggregate data for 3 cell replicates with varying potential limits for regeneration treatment indicating partial dependence of recovery ratio on recovery from prior treatment.

a

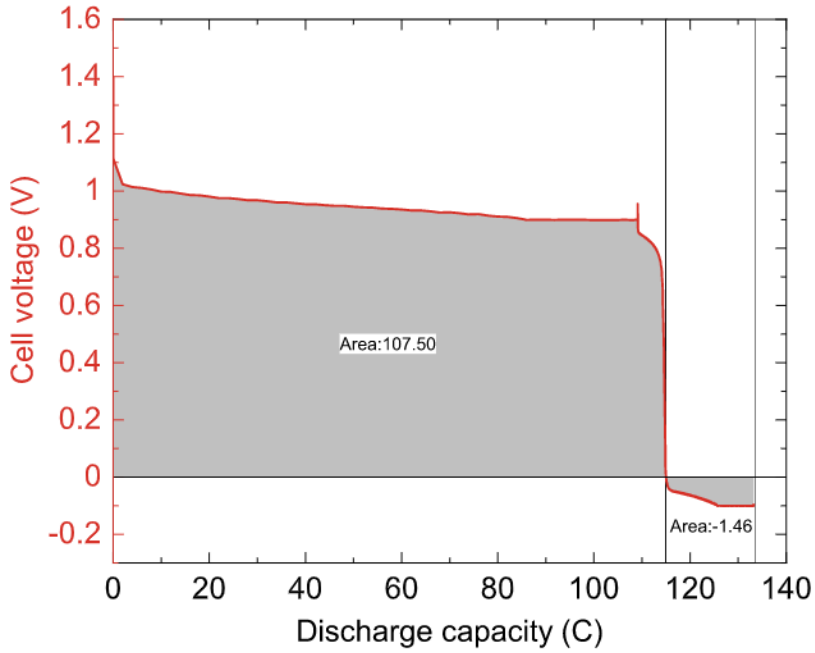

b

Cycle number	Area above 0 (V · C)	Area below 0 (V · C)	Area ratio |below/above|×100 (%)
52	108.53	-1.29	1.18
103	107.50	-1.46	1.35
154	107.53	-1.51	1.50
205	105.50	-1.36	1.29
256	105.62	-1.41	1.33
307	103.82	-1.34	1.29
358	103.88	-1.34	1.29
409	103.15	-1.22	1.18
460	103.05	-1.22	1.18
511	102.91	-1.30	1.26
562	104.52	-1.37	1.31
613	103.93	-1.38	1.33
664	102.72	-1.38	1.34
Average	**104.82**	**-1.37**	**1.30**

Extended Data Fig. 3 | Energetic cost of electrochemical regeneration in Fig. 4a and c. a, Integrated areas above and below 0 V of the cell discharge voltage profile with electrochemical regeneration in Fig. 4c. **b**, Integrated areas above and below 0 V of the cell discharge voltage profiles with 13 regeneration processes in Fig. 4a. The area ratio (%) represents the percentage of discharged electrical energy that is subsequently used for regeneration during a single discharge process, reflecting the energetic cost. It is, on average, 1.30%. Note that the electrochemical regeneration step is not performed in every cycle, but rather once every 51 cycles. Relative to the total electricity discharged during 51 cycles, the energetic cost for regeneration is only 0.025%.

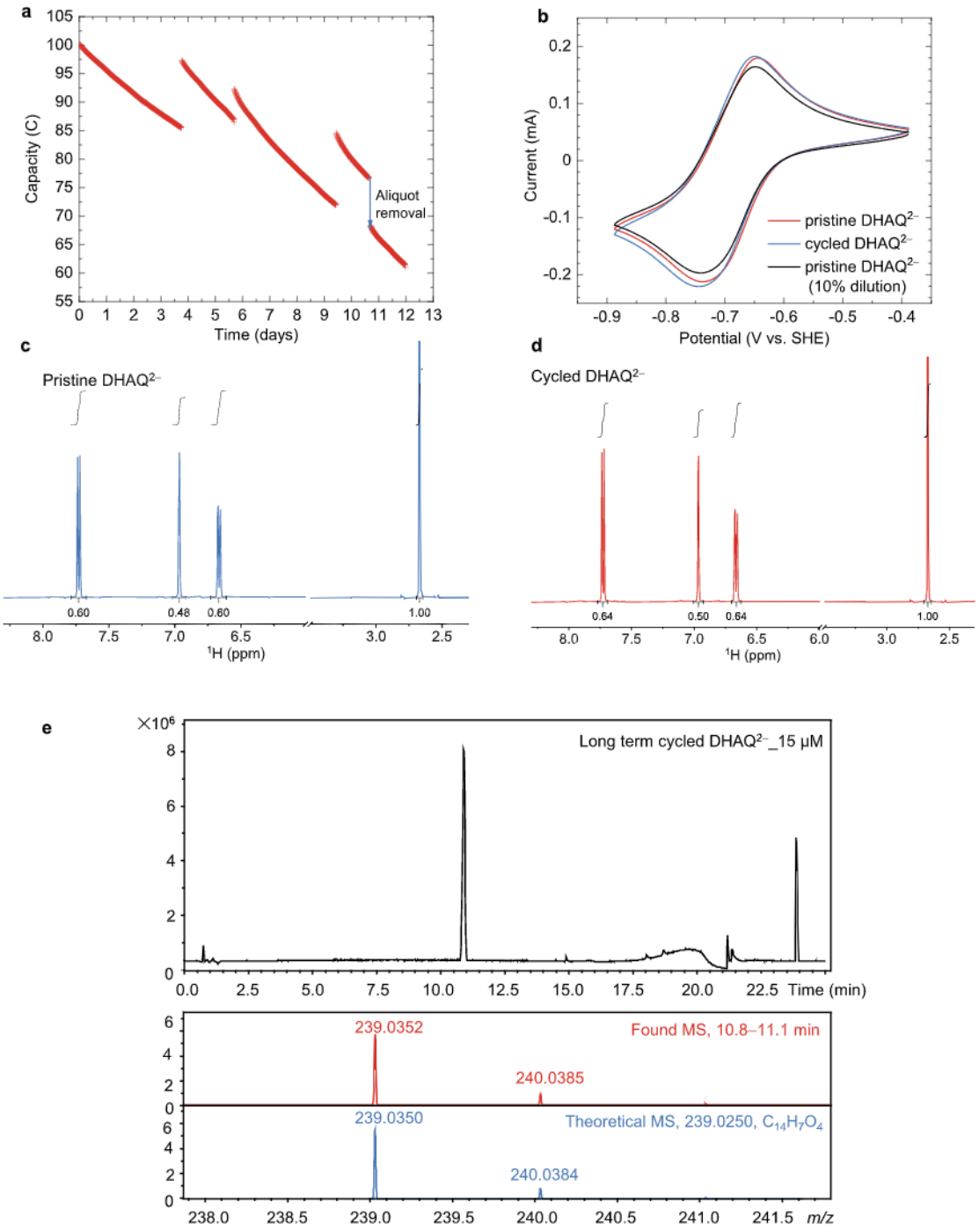

Extended Data Fig. 4 | DHAQ concentration tracking. a, Cycling of battery composed of 5 mL 100 mM $DHAQ^{2-}$ in the negolyte and 20 mL of a mixture of 100 mM $K_4[Fe(CN)_6]$ and 50 mM $K_3[Fe(CN)_6]$ in the posolyte. Galvanostatic cycling at ±50 mA/cm² with potential holds at 1.0 V and 1.5 V and current cutoff of ±1 mA/cm² during normal cycles. Three electrochemical oxidation treatments before an aliquot was removed from negolyte reservoir on day 10 for concentration measurement. **b**, Cyclic voltammograms of 20 mM $DHAQ^{2-}$ in 1 M KOH on glassy carbon working electrode. Pristine $DHAQ^{2-}$ electrolyte measured before and after dilution by 10% to verify resolution of measurement. Cycled $DHAQ^{2-}$ data refers to an aliquot removed from negolyte in part a, after ~25% capacity had been lost. No change in peak current suggests $DHAQ^{2-}$ concentration has not changed during cycling after regeneration treatment. **c & d**, Comparison of $DHAQ^{2-}$ NMR peak integral with respect to DMSO internal standard. Similarity of the peak integral of cycled electrolyte which had lost ~25% of capacity to that of pristine $DHAQ^{2-}$ does not indicate overall decrease in $DHAQ^{2-}$ concentration. An aliquot of the cycled $DHAQ^{2-}$ was taken for ^1H NMR measurement when ~25% capacity was lost on day 10.5. **e**, LC–MS result of the cycled $DHAQ^{2-}$. The peak at 10.8–11.1 min is from $DHAQ^{2-}$, which is the sole compound detected. Other peaks are from background, which can be ignored.